Accurate Numerical Flow Simulation of Hovering Rotors using different Transition Prediction Methods

C. C. Heister	J. Raddatz	A. Klein
DLR Braunschweig	DLR Braunschweig	University of Stuttgart
Germany	Germany	Germany
christoph.heister@dlr.de	jochen.raddatz@dlr.de	klein@iag.uni-stuttgart.de

ABSTRACT

In order to numerically determine the laminar-turbulent transition on hovering rotors, the applicability of three different prediction methods originating from fixed wing applications has been investigated. This includes the AHD method, used with approximated boundary layer data, and the Drela e^N envelope method, using integral boundary layer parameters. Both methods are implemented in the structured flow solver FLOWer. Furthermore, a boundary layer / e^N stability code coupled to the hybrid flow solver TAU was taken into account. One two-dimensional test case (Somers airfoil) and two three-dimensional hovering rotor test cases (ONERA 7A rotor and DLR Bo 105 flight test) serve to test and validate predicted transition and its influence on rotor performance.

1.   INTRODUCTION

CFD has been gaining popularity in helicopter research and development over the last decade. At the present time, CFD analysis based on the solution of Reynolds-Averaged Navier-Stokes (RANS) equations is being used in industry to study isolated helicopter components like the main rotor, the rotor hub or the fuselage.

But there is still a strong need in the design offices to get more robust and more accurate results from the numerical simulation tools, especially for performance predictions. Similar to fixed wing aircrafts, the modeling of the laminar-to-turbulent transition is a crucial issue when high quality results for rotor blades are sought. It is known, e.g. from in-flight experiments in 1987 on a BO 105 in hover condition [1], or from in-flight experiments on a Dauphin aircraft presented in [2], that there exist significant laminar flow regions on the blade surface of a hovering rotor. In both experiments, visualization of the flow on a helicopter rotor blade has been performed using acenaphthen.

Airfoils currently used for helicopter rotors, like the OA series in France or the DM-H-series in Germany, already exhibit wide operating limits for laminar boundary layers in order to reduce the viscous drag and improve therewith the aerodynamic performance of the rotor blade. Developing the next generation helicopters, there is a strong need to improve environmental performance, reducing the noise and the emissions. Therefore, the next generation rotor blades will have advanced tip shapes, potentially active trailing edge flaps and of course new airfoils with improved lift over drag ratio, among others achieved by delayed transition. It is obvious that the accurate numerical performance prediction of such a rotor requires an accurate RANS solver including transition prediction.

This paper will present the first steps at DLR and University of Stuttgart towards adapting transition prediction methods, which have been developed and validated for 2D and 3D fixed wing applications, for a helicopter rotor in hover. The future objective of this approach is the application of the transition prediction methods on rotors in forward flight conditions. Therefore, the main focus of this study is to identify methods which are robust and fast, using standard mesh densities.

The paper will present results for hovering rotors with different transition prediction methods, on the one hand empirical and semi empirical transition criteria integrated into DLR's structured

RANS solver FLOWer [3] and on the other hand computational results obtained with DLR's hybrid RANS solver TAU [4], which offers the possibility to predict the laminar turbulent transition location using a boundary layer code and an e^N stability code [5].

The computations are performed for the BO 105 rotor for comparison with the flow visualization in-flight experiments from 1986 and for the 7A rotor, where transition data developed from calculations with a coupled Euler / boundary layer method performed at ONERA are available [2].

2. NUMERICAL METHODS

The DLR software packages FLOWer and TAU solve the time dependant, three dimensional, compressible, Reynolds averaged Navier-Stokes (RANS) equations on block-structured (FLOWer) and hybrid grids (TAU), respectively. Details are given in [3] and [4]. They have been particularly designed for industrial aeronautical applications, thus providing Chimera for treating complex geometries. A variety of turbulence models is available in both codes ranging from simple algebraic eddy viscosity models over one and two equation models up to algebraic stress models. For the results presented within this paper the Menter к-ω SST model [6] - a two equation eddy viscosity model developed for aeronautical aerodynamics – has been applied.

The numeric of FLOWer and TAU is based on a Finite Volume method, providing a variety of spatial discretization schemes. For the computations here, a central scheme of second order accuracy, using artificial dissipation, has been employed for discretizing the RANS equations. The turbulence equations are discretized by a first order upwind scheme. In FLOWer the RANS equations are integrated by a five-stage Runge-Kutta scheme, which is accelerated by local time stepping, implicit residual smoothing and multigrid. However the turbulence equations are integrated by an implicit DDADI scheme on the finest grid level only. In TAU, the equations are integrated either by an implicit LUSGS scheme or an explicit Runge-Kutta scheme, where again multigrid acceleration can be applied to the RANS equations.

3. TRANSITION PREDICTION

To predict transition on rotors at hover, two different approaches will be investigated:

- an internal boundary layer approach using the FLOWer solver with semi-/empirical criteria (AHD and Drela e^N envelope method),

- an external boundary layer approach using the TAU solver in combination with a boundary layer and stability code (e^N);

Internal boundary layer approach using FLOWer

The internal boundary layer approach of FLOWer uses a transition prediction algorithm which is directly implemented into the flow solver. It is hereby part of the iterative solution process and utilizes the RANS solution of the boundary layer flow. Evaluation of the boundary layer is done along grid lines, compatible with static or moving meshes. Assuming an airfoil or wing like geometry, the prediction algorithm operates on defined sections in span wise direction, as schematically shown in *Figure* 1.
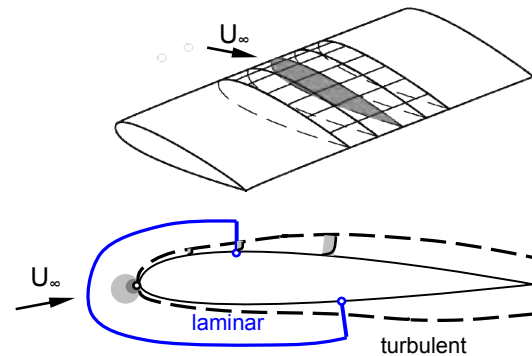

Figure 1.   *Schematic of transition prediction algorithm in FLOWer.*

The prediction algorithm will subsequently be executed in user defined intervals of iteration cycles for each span wise section. Upon execution, the following basic steps will be run through:

1. Detection of stagnation point.
2. Detection of laminar separation.
3. Detection of boundary layer edge.

4. Evaluation of boundary layer parameters.

5. Evaluation of transition criterion.

6. Initialization of laminar/turbulent flow regions via 'ltflag' parameter.

The organization of the above algorithm is based on experiences gained with e^N methods, as previously shown in [7]. Stagnation point detection is realized as search for the global pressure maximum in chordwise direction. Boundary layer thicknesses will be evaluated either from the velocity profiles or as approximate values, depending on the employed criterion. As a result of the criterion's evaluation process, transition onset positions for the section's upper and lower side will be set. A zone of laminar flow will then be initialized in upstream direction relative to the detected onset point. The laminar-turbulent transition is modelled using a ramping function.

3.1 AHD criterion and laminar separation

The AHD criterion combines the consideration of longitudinal Tollmien-Schlichting instabilities as well as effects of the free stream's turbulence level [8]. For the computations conducted with the AHD criterion, the momentum and displacement thickness will be approximated according to Thwaites and Prandtl [9]. The intention is, to become independent of a boundary layer edge detection method, often leading to numerical instabilities. Furthermore, transition prediction can be conducted, even on meshes with poor boundary layer resolution. Since the AHD criterion is defined for attached laminar flow, a second criterion checks the boundary layer for laminar separation. The criterion is defined as flow reversal near the wall. The presence of a positive pressure gradient is additionally taken into account to avoid accidental stagnation point detection. A detected location of a laminar separation will serve as a location of transition onset until the next prediction step is executed.

3.2 e^N envelope method

The e^N method, first developed by Smith and Gamberoni [10] and van Ingen [11], is based on linear spatial stability theory. Integration of the amplification rates for each frequency starting from the primary instability point yields the amplification factor n. Transition of the laminar boundary layer is then assumed at the stream-wise position at which the most dominant Tollmien-Schlichting wave reaches a critical amplification factor. Its value is assumed to mainly depend on the turbulence level of the onflow as well as the surface quality. In a simplified approach, only the envelope of the amplification curves is considered, with a loss of information about the frequency content. The e^N envelope criterion however is able to predict transition within a laminar separation bubble since the considered kinematic shape factor is a representative boundary layer parameter. The current implementation in FLOWer closely follows the work of Drela [12] who used correlations of the envelope slope and the primary instability point with the local kinematic shape factor and the momentum thickness Reynolds number based on Falkner-Skan profiles. The exact correlations are left out for brevity, but are in accordance with the transition prediction implemented in Drela's XFOIL version 6.96 [13].

3.3 Boundary Layer code plus e^N-database method

The transition prediction module of the TAU code applies a laminar boundary layer method for a fast and highly accurate computation of the laminar boundary layers. The TAU code communicates the surface Cp-distribution as input data to the laminar boundary-layer code [20], which computes the boundary layer parameters needed for the stability code LILO [21]. Based on the stability analysis done by LILO, e^N-methods for Tollmien-Schlichting and cross flow instabilities determine transition locations that are communicated back to the TAU code. This coupling structure results in an iteration procedure for the transition locations within the iterations of the RANS equations. The structure is outlined graphically in Figure 2.

During the computation, the TAU code is stopped after a certain number of iteration cycles usually when the lift or thrust in case of rotor calculations has sufficiently converged, the

transition module is called and transition points are determined and fixed in the computational grid. This is done consecutively for all upper and lower sides of all specified wing or rotor blade sections which are defined along grid lines or by 'line-in-flight' cuts. When all transition locations have been communicated back, each transition location is slightly underrelaxed to damp oscillations in the convergence history of the transition points. Then, all underrelaxed points – they represent a transition line on the upper or lower surface of a wing element in form of a polygonal line – are mapped onto the surface grid and the computation is continued.
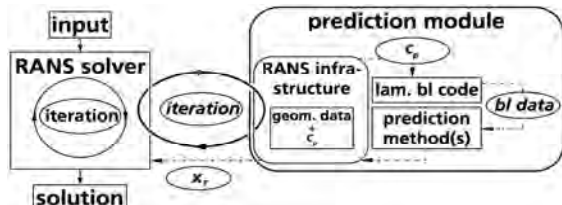
Figure 2.   Coupling structure of the RANS solver TAU and the transition prediction module [5].

In favour of the presentation of the current results the authors refer to the references [5] and [22] - [25] for further and much more detailed information on the transition coupling, the backgrounds of its construction and its different application modes.   For the application of the TAU code and the transition prediction approach described above, the method – originally developed for a wing and transport airplane applications –- has been used without any modification for rotor simulations.

4.   APPLICATIONS

Three test cases will be presented, demonstrating the application of the different transition prediction methods.   This includes a natural laminar flow airfoil and two rotor test cases at hover, conducted as stationary computations.

4.1   2D validation case

For basic validation, the transition criteria are used to predict transition onset for a two-dimensional natural laminar flow airfoil, the so

called 'Somers airfoil' NLF(1)-0416 [17]. The computational flow conditions correspond to a low Mach number flow at M= 0.1 and a Reynolds number of Re= $4.0 *10^6$. Angles of attack vary in the range from -4° to +14° to cover the experimental data. The FLOWer computations for the AHD and the Drela e^N envelope method are performed on a single block C-mesh with 337x72 points and a boundary layer resolution of approximately 40 points.
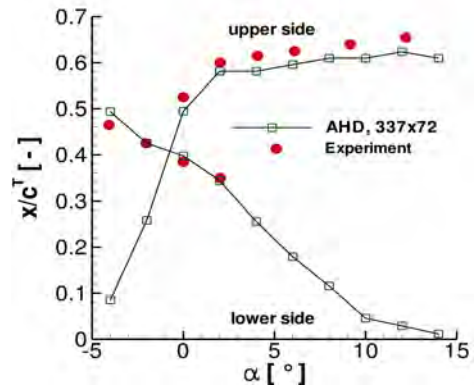

Figure 3.   Somers airfoil – experimental and computed onset positions (AHD).

The onset positions predicted with the AHD criterion are shown in Figure 3. As can be seen, the trend of the experimental data is closely captured. The average offset is 2% of chord length in upstream direction. Thus, the AHD criterion in combination with approximated boundary layer parameters gives reasonable results here.
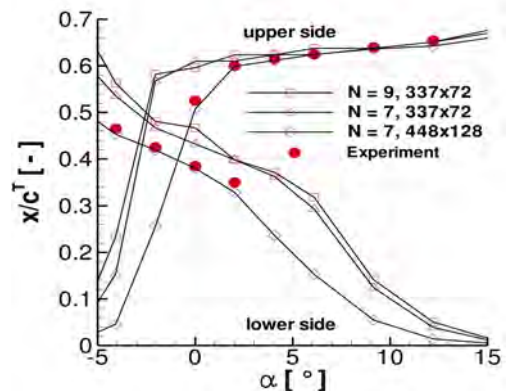

Figure 4.   Somers airfoil – experimental and computed onset positions (Drela e^N envelope).

Figure 4 shows the calculated onset positions for the Drela e^N method as evaluated from the Navier Stokes boundary layer profiles. Since no information of the turbulence intensity for the wind tunnel measurements is available, calculations with several critical amplification factors were run. On the coarse grid, transition onset is generally predicted slightly more downstream compared to the experiment. A critical amplification factor N=7 on a refined grid (448x128 points) leads to a very good match with the wind tunnel measurements, with an average upstream offset of 1% chord length.
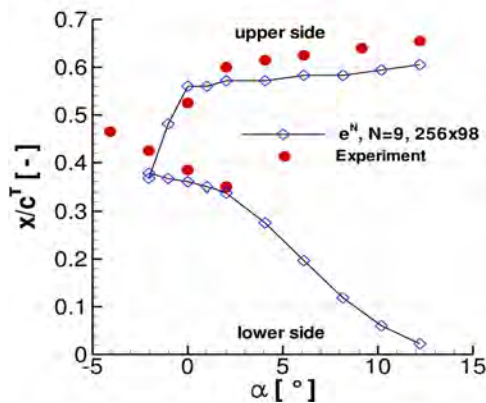
Figure 5.   *Somers airfoil – experimental and computed onset [18] (boundary layer plus e^N method).*

Results for the external boundary layer approach with TAU in combination with the e^N method are shown in Figure 5 for a range of -2° to 12°. An unstructured O-grid consisting of 25.000 tetrahedrons was used, resolving the boundary layer with 256x65 points. Comparison with experiment is close, showing minimal upstream deviations.

4.2   7A rotor in Hover

The ONERA 7A rotor is a four-bladed, fully articulated, Mach scaled model rotor with a radius of 2.1 meters. The blades with an aspect ratio of 15 have a rectangular planform shape and are made of OA2XX airfoils with varying thickness from 13 to 9 percent. The hover tests using a tip Mach number of 0.617 have been performed in the Marignane outdoor facility at EUROCOPTER. The rotor was not instrumented

so that experimental data, presented e.g. in [2], consist of rotor total performance data (thrust, power and figure of merit as a function of collective pitch).

The structured grids represent only one blade and cover an azimuthal section of 90 degrees. The influence of the other blades is taken into account by periodicity boundary conditions. The grids have a C-H monoblock topology with 217 points in the chordwise direction, 61 points in spanwise direction (with 33 points on the blade) and 57 points in the direction orthogonal to the blade surface. Grids were generated for 3 different values of the collective pitch angle θ_c: 5.97°, 7.46° and 8.94°. The structured grids were used for the computations with both codes, for the block structured code FLOWer as well as for the hybrid code TAU.

According to Ref. [2] the torsion deformation of the 7A rotor is small and there was no influence on the computed figure of merit observed. Therefore, the aerodynamic characteristics of the 7A rotor were computed assuming the blades as rigid bodies.
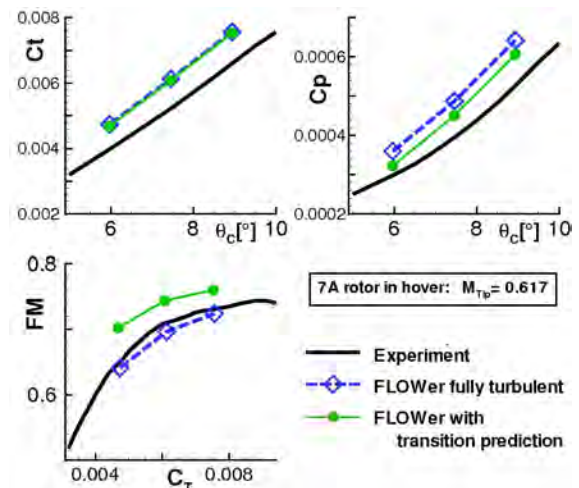

Figure 6.   *Comparison of FLOWer computations with experiment for the 7A rotor (thrust, power and FM).*

The computed thrust and power coefficients as a function of collective pitch are presented in Figure 6 with open symbols for the fully turbulent results and closed symbols for the calculation using AHD transition prediction criteria of FLOWer. TAU results are not available as an

appropriate post processing for hovering rotors is currently missing.

In the figures, the numerical curves are compared with experimental data taken from [2]. The turbulent FLOWer results show for the thrust coefficient an overestimation between 15 % and 13 % and a quite constant overestimation for the power coefficient by 17 %. For the numerical results including consideration of laminar-turbulent transition, the agreement with experimental data has been slightly improved for the thrust coefficient and considerably improved for the power coefficient.The strong influence of the consideration of the laminar-turbulent transition on the figure of merit is also shown clearly in Figure 6.

A global view of the flow conditions on the 7A rotor blade at $\theta_c = 8.84°$ is shown in Figure 7 representing the pressure distribution computed by TAU and the transition locations computed by TAU (solid line) and FLOWer (dashed line). It should be mentioned again, that the transition prediction method of the TAU code has been used the first time for a hovering rotor simulation. With exception of the correct normalization of the pressure data no further adaptations have been introduced.
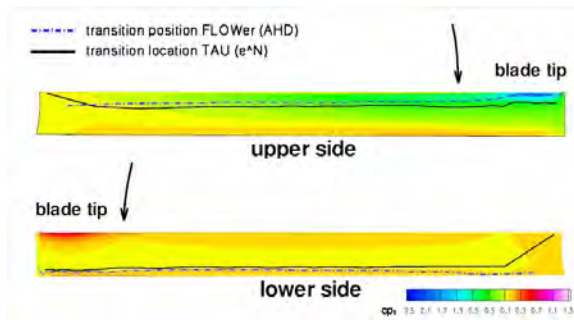

Figure 7.　7A rotor: computed pressure distribution and transition locations.

A detailed comparison of numerical pressure distributions and transition locations for the same case is shown in Figure 8 for 4 different 2D slices. The numerical pressure distributions show a good agreement. The behaviour of the predicted transition locations differs on upper and lower side. On the lower side the predicted locations are close together and very close to the minimum pressure. However, on the upper

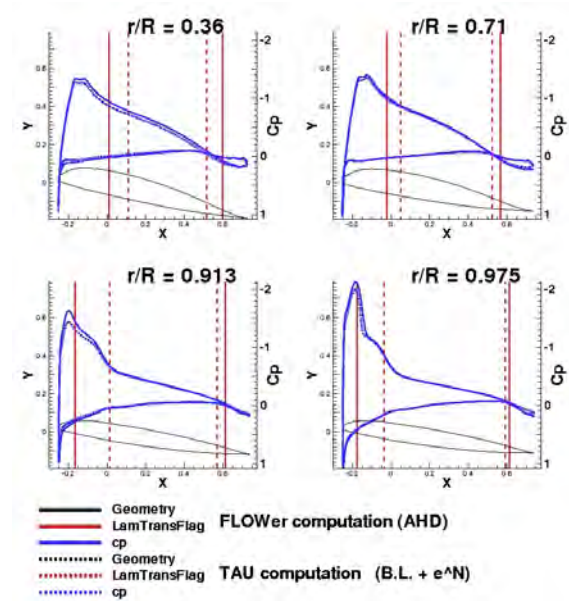side the TAU results are shifted more downstream.

Figure 8.　2D slices of the 7A rotor with numerical pressure distributions and predicted transition locations.

Figure 9 shows a comparison of the transition locations for the 3 different collective pitch angles including the results from ONERA (see Ref. [2]), using a coupled Euler / Boundary Layer method.
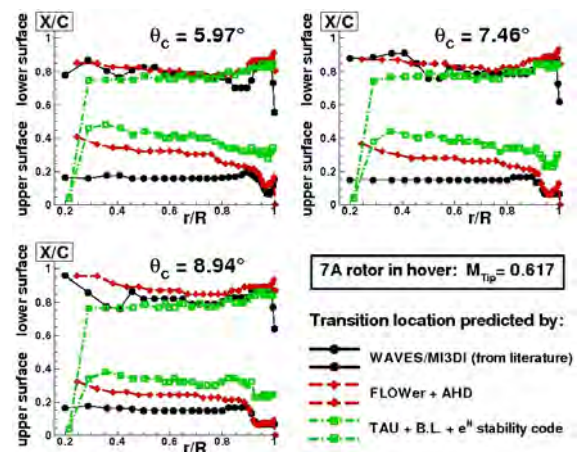

Figure 9.　7A rotor in hover: comparison of predicted transition locations on upper and lower blade surface.

Again, the predictions of the 3 different methods agree well on the lower blade surface and show quite large differences on the upper surface.

4.3 BO 105 in Hover

The presented validation case for a hovering rotor refers to a flight test conducted at the DLR in 1986 with a Bo 105 helicopter [1].
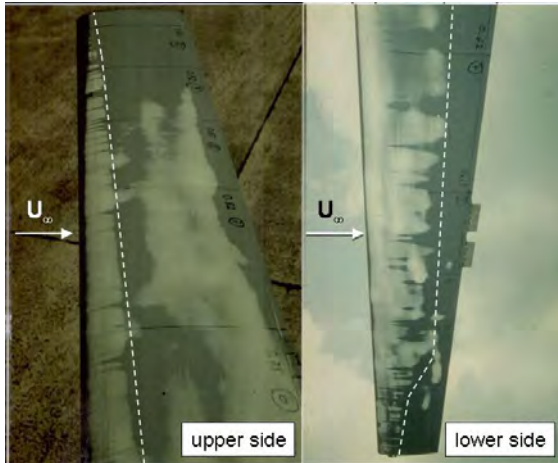

Figure 10. Bo 105 flight test – acenaphthen coating, indicating areas of laminar flow (light areas) [1].

To identify regions of laminar flow on the main rotor, one blade was coated using acenaphthen. The coating covered an area ranging from 62% blade radius to the tip, including the blade's upper and lower side. Transition onset was determined by visual interpretation of the sublimated areas. Figure 10 shows exemplary photos taken after the flight experiment. Looking on the upper side, transition sets in at approximately 20% chord length, while on the lower side onset can be observed at 70% chord continuously shifting upstream to 40% with increasing blade radius.

The flight experiment is simulated using an isolated rotor. Atmospheric conditions according to ISA at sea level are assumed, together with a typical TOW of 2250kg. Table 2 summarizes the main operating and free stream conditions. The grid topology consists of a child grid, representing the blade's geometry, and a background grid, covering a section of 90° azimuth to represent the four bladed layout of the main rotor. Two child grids have been

generated; featuring a coarse and a medium resolved boundary layer (see Table 1).

Grid points	tangential	normal	BL
coarse	145	41	~15
medium	193	65	~40

Table 1. Bo 105 child grid – resolution of airfoil surface.

The radial resolution of the blade is held constant with 97 points. A NACA 23012 airfoil contour is used, modified by a tab at the trailing edge to represent the actual airfoil geometry. The blade's main geometric characteristics are identical with the original blades of the BO105 helicopter.

Ω	44,5 rad/s
V_{TIP}	218,05 m/s
M_{TIP}	0,64
R_{TIP}	4,03E6
T_∞	288,15 °K
p_∞	101300,0 Pa
c_T	0,0050

Table 2. Bo 105 main rotor – conditions for hovering flight.

Periodic boundary conditions are defined at the azimuthal block faces of the background grid. Characteristic variables and Froude boundary conditions are used at the inlet, outlet and outer radial face of the computational domain. The inner radial face is defined as EULER slip wall. An overview of the subsequently investigated cases is given in Table 3.

Grid	Method	Blade structure
coarse	AHD	rigid
coarse	AHD	deformed
medium	AHD	deformed
medium	e^N envelope	deformed

Table 3. Bo 105 hover case - overview of investigated prediction methods.

Coarse grid solution: AHD, rigid/elastic blade

The hover computations are trimmed for a thrust coefficient of $c_T = 0.0050$. The first computation uses the AHD criterion, assuming a rigid blade with a precone angle of 2.5°. Figure 11 shows the resulting transition distribution over the blade's surface.
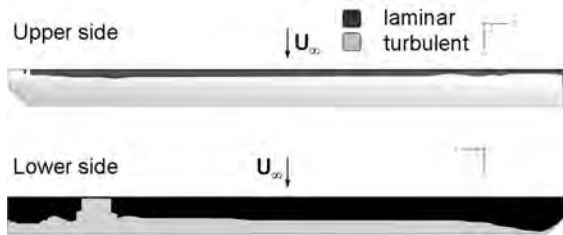

Figure 11. *Bo 105 main rotor – predicted onset (AHD, rigid blade, coarse grid).*

On the upper side, a nearly constant onset at approximately 20% can be observed. Transition is triggered by positive pressure gradients, downstream of chord wise suction peaks (see Figure 12). On the blade's lower side, the pressure distribution shows moderate positive gradients, with prolonged laminar running lengths of approximately 65% chord length.
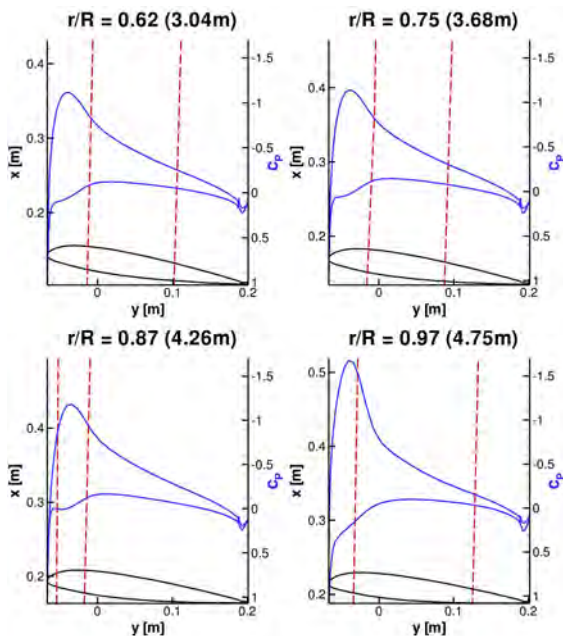

Figure 12. *Bo 105 main rotor: c_p-distributions (AHD, rigid blade, coarse grid).*

Computed and experimental onset positions are compared in Figure 13. On the upper side agreement with flight test data is close, with an average upstream offset of 4% chord length.
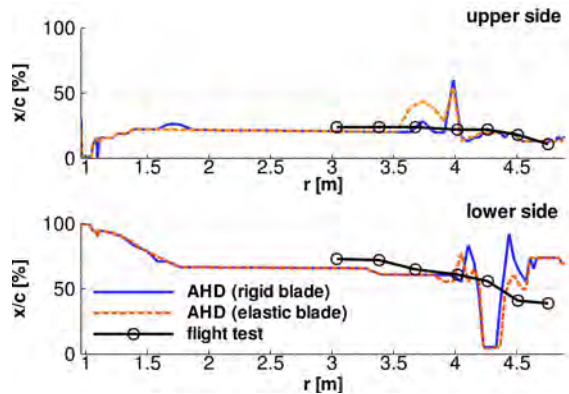

Figure 13. *Bo 105 main rotor – computed and experimental onset (coarse grid).*

On the lower side, the computation is in close agreement up to $r/R = 85\%$ ($r = 4.2$ m). At $r/R = 87\%$ ($r = 4.3$ m), transition occurs near the leading edge, caused by local suction peaks on the lower side. This blade section happens to be influenced by the periodic wake shed by the rotor (see Figure 14).
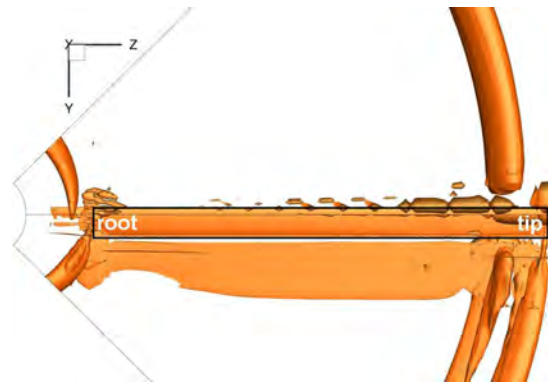

Figure 14. *Bo 105 main rotor – top view of rotor wake (λ_2 criterion, iso-surfaces).*

The vortical flow structure induces an area of locally reduced pressure near the leading edge. Transition is subsequently triggered by the disturbed pressure distribution. However, the wake's influence on transition onset can not be observed in the flight test data. Looking on the lower side (see Figure 13), computed laminar areas near the blade tip generally extend up to

75% chord, while experimental onset occurs at 40%.

A second computation is performed to investigate the influence of the blade's elastic behaviour on the onset distribution, especially near the tip. Therefore, a coupled FLOWer / HOST [19] computation is done, using a beam model to represent the blade's structural characteristics.
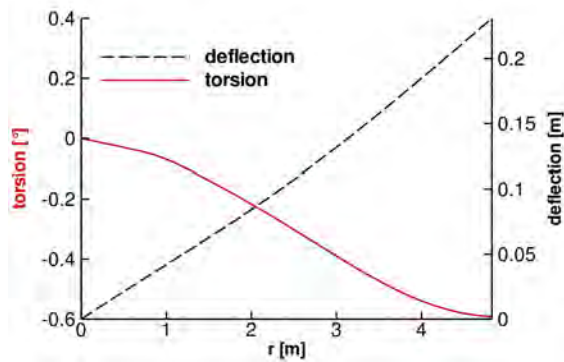

Figure 15. Deflection and torsion of the c/4 line - HOST [19] beam model.

Trimming for c_T=0.0050, the resulting elastic properties of the blade's c/4 line are shown in Figure 15. A moderate nose down twist due to torsion can be observed, tending to locally reduce the aerodynamic angle of attack and hence shorten laminar running lengths on the lower side. However, taking into account the elastic deformation does not lead to a noticeable effect on transition onset prediction, as can be seen in Figure 13. The computed transition lines for the elastic and rigid case only show minor deviation to each other.

Medium grid solution: AHD, deformed blade

A further AHD computation is conducted on a mesh with medium boundary layer resolution. The blade's elastic behaviour is accounted for by imposing the deformation of the previous trimmed calculation (see Figure 15) on the grid's coordinates. The thrust coefficient converges to c_T = 0,0051, which is in good accordance with the target value. Predicted laminar areas are shown in Figure 16. Laminar areas extend up to 20% on the upper side, and 65% on the lower
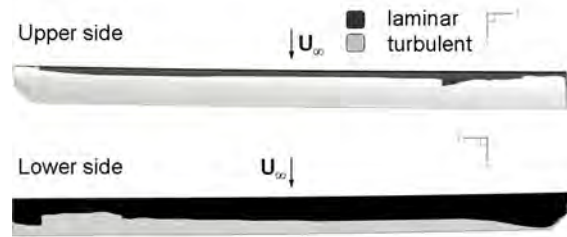
side.

Figure 16. Bo 105 main rotor: predicted onset (AHD, deformed blade, medium grid).

The comparison with flight test data reveals a generally close agreement, as shown in Figure 17. Noticeable improvement of prediction accuracy occurs on the blade's lower side, near the tip at r/R = 87% (r = 4.3 m). While the coarse grid solution locally shows sudden transition near the leading edge (see Figure 13), laminar flow on the medium grid extends up to 50% chord length, close to the flight test measurements. Since onset positions in this region are predicted via laminar separation, the improved mesh quality obviously improves the accuracy for this particular criterion.
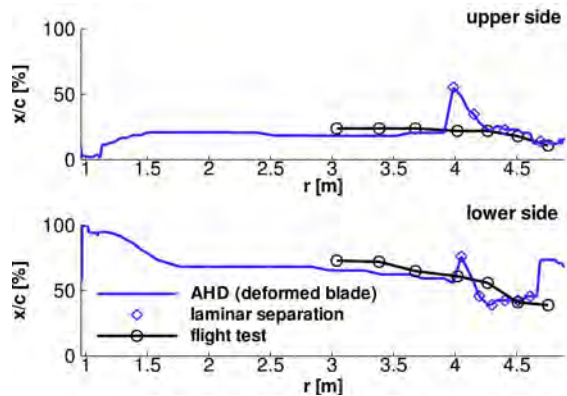

Figure 17. Bo 105 main rotor: computed and experimental onset (medium grid).

For sections located inboard of r/R = 82% (r = 4.0 m), transition is predicted by the AHD criterion due to longitudinal instabilities. The onset positions are found to be located downstream of the pressure minimum, as can be seen in Figure 18.
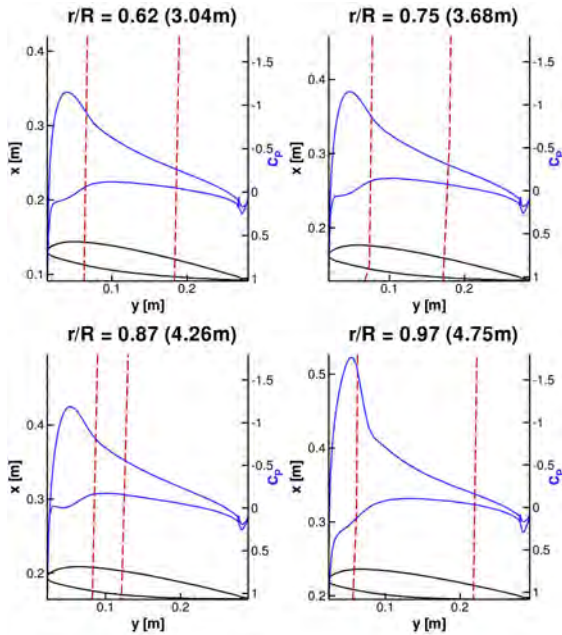
Figure 18. Bo 105 main rotor: c_p-distributions (AHD, deformed blade, medium grid).

Medium grid solution: e^N envelope method, deformed blade

A calculation on the medium grid was performed to investigate the applicability of the Drela envelope method for the Bo 105 hover case. Figure 19 shows the resulting transition distribution over the blade's surface for a critical amplification factor of n_{crit}=12, which is generally associated with undisturbed freestream conditions.
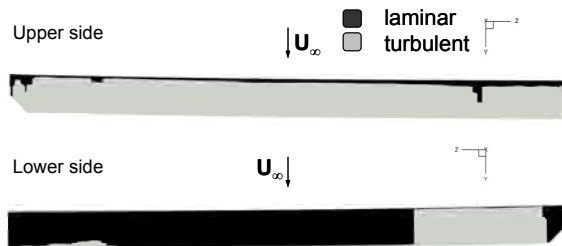

Figure 19. Bo 105 main rotor – predicted onset (Drela e^N envelope, deformed blade, medium grid).

On the upper side, transition onset takes places at approximately 5-15% along most of the blade span. On the lower side, the method largely fails

to give meaningful results predicting laminar-transition practically either at leading or trailing edge. As shown in Figure 20, while the pressure distribution is accurate and equivalent to that of the AHD criterion (compare to Figure 18), the transition locations do not fit. On the upper side, transition even occurs during flow acceleration.
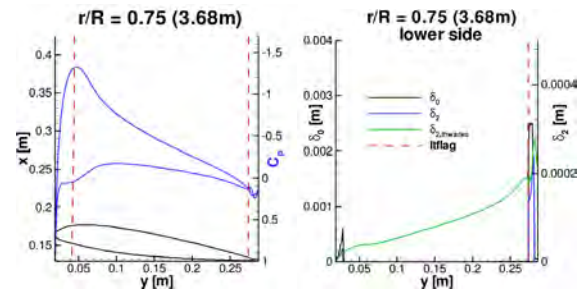

Figure 20. Bo 105 main rotor – left: c_p-distribution, right: boundary layer quantities (Drela e^N envelope, deformed blade, medium grid).

A more detailed investigation showed that the calculation of the boundary layer quantities failed during the computation. Taking a look at the calculated boundary layer on the blade's lower side, also depicted in Figure 20, jumps can be observed in the boundary layer thickness δ_0 and the momentum thickness δ_2.

The implemented boundary layer detection, according to Stock and Haase [26], is obviously not able to identify the boundary layer edge correctly on the given grid density, leading to errors in all other boundary parameters and thus in the transition prediction. It can further be seen that the Thwaites approximation, which is used for the AHD criterion, on the other hand still delivers a robust streamwise momentum thickness development. However, since the envelope method further involves the displacement thickness of the boundary layer, using this empirical relation does not offer a solution. It is believed that both the missing robustness of the implemented boundary layer edge detection as well as the quite coarse grid resolution contribute to the unsatisfactory behaviour of the e^N envelope prediction method. Further studies will be performed towards a more reliable application of this criterion in the future.

- 10 -

5. CONCLUSION

With the main objective to gain more accurate performance predictions from numerical rotor simulations, the currently available methods at DLR and University of Stuttgart to consider the laminar-turbulent transition location have been investigated. Tests with three different methods were performed for a 2D case and two different hovering rotor cases. These include the AHD method with approximated boundary layer data, the Drela e^N envelope method with integral boundary layer profiles and an approach using a CFD solver coupled with a boundary layer and an e^N stability code.

For a laminar flow airfoil, computed onset positions were in close agreement with the experiment for all methods. For the 7A rotor under hover conditions, the AHD criterion and the e^N stability code are compared to results from literature, computed at ONERA using a coupled Euler/boundary layer method. All methods show a good agreement for the predicted transition locations on the lower blade surface. However, on the upper surface the results are spread over a wide range between 20 and nearly 40% of chord length and require a further investigation. A strong influence of the correct representation of laminar-turbulent transition location on the power coefficient and the figure of merit has been found.

A flight test performed with a BO 105 helicopter at DLR served as second hover validation case. Comparison of the computed AHD results to flight test data are generally in close agreement. Refinement of the grid resolution positively influences the correlation with flight test data in the tip region. The consideration of elastic blade deformations shows only small effects on the computed onset positions. However, they have to be taken into account for accurate performance predictions.

Generally, the application of transition prediction methods, which have been developed for fixed wing applications, gives reasonable results for hovering rotors. A robust and reliable evaluation of the boundary layer parameters has to be assured, since computations are conducted with medium grid resolutions to maintain reasonable computational effort. Appropriate methods for BL edge detection should be identified, besides using approximations or external BL codes. The robust provision of BL data will be a key topic looking towards instationary applications, like rotors in forward flight.

For a final assessment of the different prediction methods, a more detailed validation is necessary, which requires accurate and well documented experimental data, including pressure distributions and recorded blade deformations.

REFERENCES

[1] C.H. Rohardt: "Flow Visualization on a Helicopter Rotor in Hover Using Acenaphthen", 13th European Rotorcraft Forum, Arles, France, 1987.

[2] P. Beaumier, E. Chelli, K. Pahlke: "Navier-Stokes Prediction of Helicopter Rotor Performance in Hover including Aero-elastic Effects ", American Helicopter Society 56th Annual Forum, Virginia, 2000.

[3] J. Raddatz, J. Fassbender: "Block Structured Navier-Stokes Solver FLOWer", *MEGAFLOW – Numerical Flow Simulation for Aircraft Design*, edited by N. Kroll and J. Fassbender, Vol. 89 of *Notes on Numerical Fluid Mechanics and Multidisciplinary Design*, Springer Verlag, 2005.

[4] T. Gerhold,: "Overview of the Hybrid RANS Code TAU", *MEGAFLOW – Numerical Flow Simulation for Aircraft Design*, edited by N. Kroll and J. Fassbender, Vol. 89 of *Notes on Numerical Fluid Mechanics and Multidisciplinary Design*, Springer Verlag, 2005.

[5] A. Krumbein, N. Krimmelbein, G. Schrauf: "Automatic Transition Prediction in a Hybrid Flow Solver, Part 1 – Methodology and Sensitivities, Part 2 - Practical Application", Journal of Aircraft, Vol. 46, No. 4, pp. 1176 – 1199, American Institute of Aeronautics and Astronautics (AIAA), 2009.

[6] F.R. Menter: "Two-Equation Eddy-Viscosity Turbulence Models for Engineering Applications", AIAA Journal, Vol. 32, No. 8, 1994.

[7] A. Krumbein: "Automatic Transition Prediction and Application to Three-Dimensional Wing Configurations", Journal of Aircraft, Vol. 44, No 1, 2007, pp. 119-133; also AIAA Paper 2006-914.

[8] D. Arnal: "Three-dimensional boundary layers: laminar-turbulent transition", AGARD Report No 741, Toulouse Cedex, 1987.

[9] B. Thwaites: "Approximate calculation of the laminar boundary layer", Aeron. Quaterly, Vol.1, 1949.

[10] A.M.O. Smith and N. Gamberoni: "Transition, Pressure Gradient and Stability Theory", Report ES 26388, Douglas Aircraft Company, 1956.

[11] J. L. van Ingen: "A Suggested Semi-Empirical Method for the Calculation of the Boundary Layer Transition Region", Report V.T.H. 71, V.T.H. 74, Delft University of Technology, Department of Aeronautical Engineering, 1956.

[12] M. Drela and M.B. Giles: "Viscous-Inviscid Analysis of Transonic and Low Reynolds Number Airfoils", AIAA Journal, Vol. 25, No. 10, pp. 1347-1355, 1986.

[13] http://web.mit.edu/drela/Public/web/xfoil/

[14] N. Kroll et al.: „Ongoing activities in flow simulation and shape optimization within the German MEGADESIGN project", 25th international congress of the aeronautical sciences, Hamburg, 2006.

[15] J.G. Leishman: „Principles of Helicopter Aerodynamics", Cambridge University press, 2nd edition, New York, 2006.

[16] W.J. McCroskey: "Measurements of boundary layer transition, separation and streamline direction on rotating blades", NASA Technical Note, NASA TN D-6321, Washington, 1971.

[17] D.A. Somers: "Design and experimental results for a natural laminar flow airfoil for general aviation applications", NASA Technical Paper 1861, Scientific and technical information branch, 1981.

[18] N. Krimmelbein, $C^2A^2S^2E$ Center for Computer Applications in AeroSpace Science and Engineering, Institute of Aerodynamics and Flow Technology, German Aerospace Center (DLR), private communications.

[19] B. Benoit et al.: "Host, a general helicopter simulation tool for Germany and France", American Helicopter Society, 56th Annual Forum, 2000.

[20] "COCO – A Program to compute Velocity and Temperature Profiles for Local and Nonlocal Stability Analysis of Compressible, Conical Boundary Layers with Suction", ZARM Technik Report, November 1998.

[21] G. Schrauf: "LILO 2.1 User's Guide and Tutorial", Bremen, Germany, GSSC Technical Report 6, originally issued Sep. 2004, modified for Version 2.1 July 2006.

[22] N. Krimmelbein, R. Radespiel, C. Nebel: "Numerical Aspects of Transition Prediction for Three-Dimensional Configurations", AIAA-2005-4764.

[23] N. Krimmelbein, R. Radespiel: "Transition prediction for tree-dimensional flows using parallel computation", Computers & Fluids, Vol. 38, 2009, pp. 121-136, 2008.

[24] A. Krumbein, N. Krimmelbein: "Navier Stokes High Lift Airfoil Computations with Automatic Transition Prediction using the DLR TAU Code", Notes on Numerical Fluid Mechanics and Multidisciplinary Design, Vol. 96, New Results in Numerical and Experimental Fluid Mechanics VI, Contributions to the 15th STAB/DGLR Symposium, Darmstadt, Germany 2006, Springer Verlag, 2007.

[25] C. Nebel, R. Radespiel, T. Wolf: „Transition Prediction for 3D Flows Using a Reynolds-Averaged Navier-Stokes Code and N-Factor Methods", AIAA-2003-3593.

[26] H.W. Stock, W. Haase: "Feasibility-Study of e^N Transition Prediction in Navier-Stockes Methods for Airfoils", AIAA, Vol.37, No. 10, p.1187-1196, 1999.